Jagannath University Journal of Science
Volume 08, Number I, December 2021, pp. 1–12
https://jnu.ac.bd/journal/portal/archives/science.jsp
ISSN 2224-1698

JnUJSci

Computational Modeling of MHD Multiphase Fluid Flow Past a Stretching/ Shrinking Sheet

Research Article

S. F. Ahmmed*, B. M. R. Haque and P. P. Gharami

Mathematics Discipline, Khulna University, Khulna-9208, Bangladesh.

Received: 22 November 2020
Accepted: 25 October 2021

Abstract: This research investigates the behavior of magneto-hydrodynamic (MHD) flow of multiphase fluid over a stretching/ shrinking sheet in the presence of nanoparticle. The considering model is made of the basic fluid governing equations such as continuity equation, momentum equation, energy equation and concentration equation. The basic governing equations are changed into dimensionless system by adopting dimensionless parameters. Then the dimensionless governing equations are solved numerically by using well known explicit finite difference method (EFDM) with the help of Compaq Visual Fortran 6.6.a which is a computer programming language. Stability and convergence analysis are discussed for the accuracy of the numerical result. The graphical representation of velocity, temperature and concentration profiles that are affected by different physical parameters. Skin friction, Nusselt number and Sherwood number are shown in graphics and tabular form. The results are discussed with the physical behavior of these parameters.

Keywords: *Multiphase fluid ● Explicit finite difference method ● Williamson nanofluid ● Chemical reaction ● MHD ● Heat and mass transfer ● Stretching/Shrinking sheet.*

1. Introduction

Multiphase fluid comprises of more than one individual component or fluid phases. Multiphase flow capable of acting the flow of two or different phases with the usual surface. Every phase shows a fragment of solid, liquid, or gaseous matter. The flow of stream and liquid are very common among various collaboration in industrial processes. In reactor engineering, a big arrangement of investigation has been executed on the class of double-phase flow due to the mislaying of coolant mishap. In fact, flows which use in a large number of the usual industrial processes are naturally multiphase flows such as liquid-particle or gas-particle suspensions used in combustion processes, pneumatic conveyors, extractors, and many processes in the chemical industry. The behavior of Multiphase fluid flow in the presence of nanoparticles passing through a stretching sheet have been analyzed by Reza-E-Rabbi et al. (2020). They investigated the behavior of multiphase Casson and Maxwell fluids with nonlinear chemical reactions. Their prime object was to characterize and establish a differentiating between Maxwell and Casson fluid in various flow fields. The impression of thermal radiation and ohomic dissipation on magneto-hydrodynamic boundary layer flow of Williamson fluid was examined by Hayat et al. (2016). Two dimensional

* Corresponding Author: S. F. Ahmmed
Email: sfahmmed@yahoo.com

steady MHD Williamson Nanofluid in presence of heat and mass fluxes was discussed by Venkatamanaiah et al. (2016). An analysis of heat and mass transfer in the presence of Lorentz force on Williamson nanofluid flow over a variable stretching sheet was introduced by Khan et al. (2018). The computational solutions are found by the shooting method. Krishnamurthy et al. (2015) discussed two-dimensional flow of MHD Williamson nanofluid over a stretching surface embedded with porous medium. A numerical analysis on variable thermal conductivity effect on flow of Carreau fluid over a sensor surface was inspected by Khan et al. (2016). They adopted shooting method for showing solutions of boundary layer momentum and heat equations. The Brownian and thermophoresis effect of the Williamson fluid flow over an unstable porous stretching surface is examined by Ali et al. (2017). They used the Homotopy Analysis Method for the exact solution and also exhibited a comparison with a numerical solution in tabular form. Reddy et al. (2017) analyzed the impact of thermophoresis and Brownian motion on unsteady magneto-hydrodynamics flow over a slandering stretching surface. They analyzed that values of Brownian motion and thermophoresis parameter increase the flow temperature, but concentration outlines decrease with rising in thermophoresis parameter. Abah et al. (2012) studied the impact of unsteady free convection flow on a vertically embedded plate with heat and mass transfer phenomena. An analysis is performed to study of heat and mass transfer effect on unsteady MHD flow of an incompressible and electrically conducting fluid by Barik (2016). The author also showed a numerical investigation of unsteady MHD flow past an isothermal vertical plate with a combined effect of heat and mass transfer. Khan et al. (2016) explored unsteady MHD radiation nanofluid flow past a stretching sheet with the help of the explicit finite difference method. Kataria and Patel (2016) have paid attention to the analytical study on MHD flow of Casson fluid over a vibrating perpendicular plate placed in a porous medium. Casson fluid passed through a vibrating perpendicular plate placed in porous medial including radiation and chemical reaction consequences was analyzed by Kataria and Patel (2016). It is seen from their study when the Casson parameter is large enough, then non-Newtonian fluid behaves like a Newtonian fluid. Hussanan et al. (2014) analyzed unsteady heat transfer flow of Casson fluid over a vast wigwag vertiginous plate using Newtonian heating. Two-dimensional steady boundary layer convective flow of Casson fluid past a horizontally embedded plate was studied by Shaw et al. (2016). Ramandevi et al. (2017) investigated MHD flow and heat lift of two sharp non-Newtonian fluids over an expanding sheet with the latest heat flux theory. Study on MHD free convection flow with variable surface over vertical plate was analyzed by Naby et al (2003). Khan et al. (2016) explored unsteady MHD radiation nanofluid flow past a stretching sheet with help of explicit finite difference method. A numerical solution of unsteady MHD flow over a semi-infinite vertical plate was presented by Loganathan (2010). Hemalatha and Bhaskar (2014) studied MHD boundary layer free convective flow with heat creation and convective frontier constrain. The laminar frontier stream of a tangent hyperbolic fluid past an upright absorptive cone was examined by Gaffar et al. (2016). Parveen and Alim (2012) deliberated the joule heating effect in presence of magnetic field of electrically conducting fluid with free convection boundary layer flow along a vertical wavy surface. In addition, a significant percentage of heat and mass transfer modeling of Newtonian and non-Newtonian nanofluids flow has been done in recent years. The following articles can be used for detailed insight (Reza-E-Rabbi et al., 2020; Abro et al., 2021; Nikan et al., 2021; Gharami et al., 2020a, 2020b)

The goal of the present analysis is to explore the heat and mass transfer flow of multiphase fluid along a porous stretching or shrinking sheet. The basic governing equations are changed into dimensionless system by adopting dimensionless parameters. Then the non-dimensional problem are calculated via explicit finite difference method (EFDM) with Fortran Language**.** The solution of the dimensionless governing equations is obtained and displayed graphically with stability analysis and convergence test.

2. Mathematical Formulation

We consider the unsteady two dimensional MHD flow of multiphase fluid past a stretching/ shrinking sheet. Here $u = ax$ be the fluid velocity and a is the stretching/ shrinking constant. When $a > 0$ then sheet is stretched and when $a < 0$ then sheet is shrunk. The fluid is flowing in x direction. Here, x axis be considered in the direction along sheet and y axis be perpendicular to surface. The flow be produced by exerting two uniform and opposing forces along x axis. An identical transversal magnetic field B_0 be set perpendicularly in flow direction and produced magnetic field be excluded because of small Reynolds number. Suppose U_w, T_w and C_w are the nanoparticle fluid velocity, temperature, and concentration near surface. Variable temperature and concentration $T_w(x) > T_\infty$ and $C_w(x) > C_\infty$, where T_∞ is the uniform ambient temperature and C_∞ is the uniform ambient concentration of the fluid.

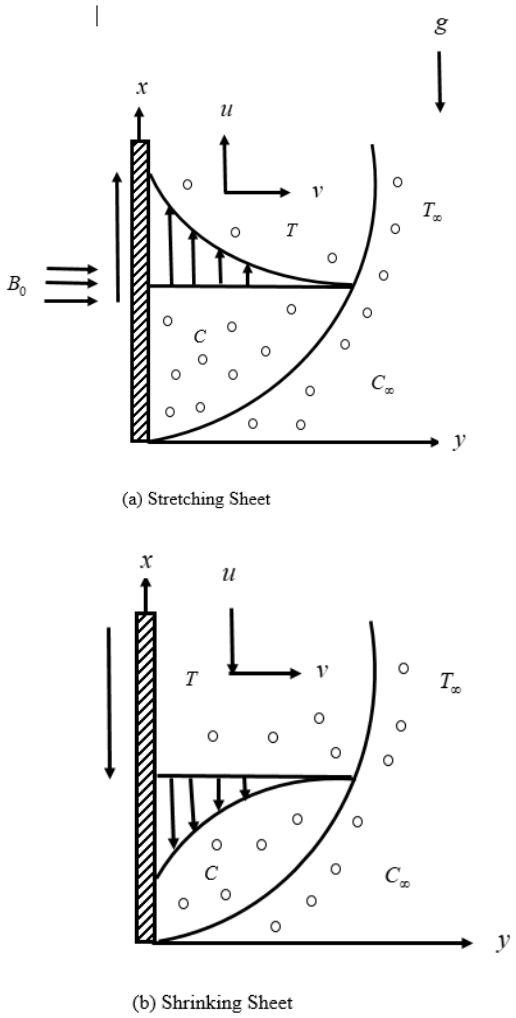

Figure 1. Physical configuration and co-ordinate system

The two dimensional governing equations i.e. continuity, momentum, energy and concentration equations are given below

$$\frac{\partial u}{\partial x}+\frac{\partial v}{\partial y}=0 \tag{1}$$

$$\frac{\partial u}{\partial t}+u\frac{\partial u}{\partial x}+v\frac{\partial u}{\partial y}=\upsilon\frac{\partial^2 u}{\partial y^2}+\sqrt{2}\upsilon\Gamma\frac{\partial u}{\partial y}\frac{\partial^2 u}{\partial y^2}-\frac{\sigma\beta_0^2}{\rho}u \tag{2}$$

$$-\frac{\upsilon}{k}u+g\beta_T(T-T_\infty)+g\beta_c(C-C_\infty)$$

$$\frac{\partial T}{\partial t}+u\frac{\partial T}{\partial x}+v\frac{\partial T}{\partial y}=\frac{K}{\rho C_p}\frac{\partial^2 T}{\partial y^2}+\frac{\upsilon}{C_p}\left(\frac{\partial u}{\partial y}\right)^2+ \tag{3}$$

$$\frac{\sqrt{2}\upsilon\Gamma}{C_p}\left(\frac{\partial u}{\partial y}\right)^3-\frac{\sigma\beta_0^2}{\rho C_p}u^2-\frac{1}{\rho C_p}\frac{\partial q_r}{\partial y}$$

$$\frac{\partial C}{\partial t}+u\frac{\partial C}{\partial x}+v\frac{\partial C}{\partial y}=D_m\frac{\partial^2 C}{\partial y^2}+\frac{D_m K_T}{T_m}\frac{\partial^2 T}{\partial y^2}-K_r\left(C-C_\infty\right) \tag{4}$$

The corresponding boundary conditions are

$$\begin{aligned} &t\le 0, u=ax, v=0, T=T_\infty, C=C_\infty \ \text{ everywhere} \\ &t>0, u=ax, v=0, T=T_\infty, C=C_\infty \ \text{ at } x=0 \\ &\quad u=ax, v=0, T=T_w, C=C_w \ \text{ at } y=0 \\ &\quad u=0, v=0, T\to T_\infty, C\to C_\infty \ \text{ at } y\to\infty \end{aligned} \tag{5}$$

Here, u and v be the velocity components in x and y direction respectively, T is the fluid temperature, C is the fluid Concentration, B_o is the applied magnetic field, β_T is the thermal expansion, β_C is the concentration expansion, υ is the kinematic viscosity, ρ is the density, K is the thermal conductivity, C_P is specific heat at constant pressure, q_r radiative heat flux, K_r is the chemical reaction, Γ is the time constant. Now utilizing Rosseland estimation, we get $q_r=-\frac{4\sigma^*}{3k_1}\frac{\partial T^4}{\partial y}$. where, σ^* be Stefan-Boltzmann constant and k_1 be average absorption coefficient. Now expanding T^4 in a Taylor series about T_∞ and ignoring higher order, we have $T^4\cong 4T_\infty^3T-3T_\infty^4$, where, T_∞ is the ambient temperature. Now energy equation reduces to the following expression:

$$\frac{\partial T}{\partial t}+u\frac{\partial T}{\partial x}+v\frac{\partial T}{\partial y}=\left(\frac{K}{\rho C_p}+\frac{16\sigma^* T_\infty^3}{3k_1}\right)\frac{\partial^2 T}{\partial y^2}+\frac{\upsilon}{C_p}\left(\frac{\partial u}{\partial y}\right)^2+\frac{\sqrt{2}\upsilon\Gamma}{C_p}\left(\frac{\partial u}{\partial y}\right)^3-\frac{\sigma\beta_0^2}{\rho C_p}u^2 \tag{6}$$

To transform the equation (1) to (6) into a set of ordinary differential equations the following dimensionless quantities are introduced

$$X=\frac{xU_0}{\upsilon},Y=\frac{yU_0}{\upsilon},U=\frac{u}{U_0},V=\frac{v}{U_0},\tau=\frac{tU_0^2}{\upsilon},\theta=\frac{T-T_\infty}{T_w-T_\infty},\phi=\frac{C-C_\infty}{C_w-C_\infty} \tag{7}$$

Taking equation (7) the dimensionless form of the governing equation (1) to (6) are

$$\frac{\partial U}{\partial X}+\frac{\partial V}{\partial Y}=0 \tag{8}$$

$$\frac{\partial U}{\partial \tau}+U\frac{\partial U}{\partial X}+V\frac{\partial U}{\partial Y}=\left[1+We\frac{\partial U}{\partial Y}\right]\frac{\partial^2 U}{\partial Y^2}-\left[M+\frac{1}{Da}\right]U+Gr\theta+Gm\phi \tag{9}$$

$$\frac{\partial \theta}{\partial \tau}+U\frac{\partial \theta}{\partial X}+V\frac{\partial \theta}{\partial Y}=\frac{1}{\Pr}\left[1+\frac{4R}{3}\right]\frac{\partial^2 \theta}{\partial Y^2}+Ec\left(\frac{\partial U}{\partial Y}\right)^2+We.Ec\left(\frac{\partial U}{\partial Y}\right)^3-M.EcU^2 \tag{10}$$

$$\frac{\partial \phi}{\partial \tau}+U\frac{\partial \phi}{\partial X}+V\frac{\partial \phi}{\partial Y}=\frac{1}{Sc}\frac{\partial^2 \phi}{\partial Y^2}+Sr\frac{\partial^2 \theta}{\partial Y^2}-Kc.\phi \tag{11}$$

The corresponding boundary conditions are

$$\begin{aligned} &\tau \le 0,\ U=0,\ V=0,\ \theta=0,\ \phi=0 && \text{everywhere}\\ &\tau > 0,\ U=0,\ V=0,\ \theta=1,\ \phi=1 && \text{at } X=0\\ &\quad U=1,\ V=0,\ \theta=1,\ \phi=1 && \text{at } Y=0\\ &\quad U\to 0,\ V\to 0,\ \theta\to 0,\ \phi\to 0 && \text{at } Y\to\infty \end{aligned} \tag{12}$$

The dimensionless parameters are given below:

Thermal Grashof number $G_r=\frac{g\beta_T\upsilon(T_w-T_\infty)}{U_0^3}$, Modified Grashof number $G_m=\frac{g\beta_C\upsilon(C_w-C_\infty)}{U_0^3}$, Magnetic parameter $M=\frac{\sigma\beta_0^2\upsilon}{\rho U_0^2}$, Prandtl number $\Pr=\frac{\mu C_P}{\kappa}$, Radiation parameter $R=\frac{4\sigma^* T_\infty^3}{k_1\kappa}$, Weissenberg number $We=\frac{\sqrt{2}\Gamma U_0^2}{\upsilon}$, Darcy number $Da=\frac{kU_0^2}{\upsilon^2}$, Eckert number $Ec=\frac{U_0^2}{C_p(T_w-T_\infty)}$, Schmidt number $Sc=\frac{\upsilon}{D_m}$, Soret number $Sr=\frac{D_mK_T}{T_m\upsilon}\left(\frac{T_w-T_\infty}{C_w-C\infty}\right)$ and Chemical number $Kc=\frac{K_r\upsilon}{U_0^2}$

The non-dimensional quantities of skin friction, Nusselt number and Sherwood number are as follows

$$Cf=\frac{1}{2\sqrt{2}}Gr^{-\frac{3}{4}}\left(\frac{\partial U}{\partial Y}\right)_{Y=0},\ Nu=\frac{1}{\sqrt{2}}Gr^{-\frac{3}{4}}\left(\frac{\partial\theta}{\partial Y}\right)_{Y=0},\ Sh=\frac{1}{\sqrt{2}}Gr^{-\frac{3}{4}}\left(\frac{\partial\phi}{\partial Y}\right)_{Y=0}$$

3. Numerical Technique

For solving the equations (8) to (12) the explicit finite difference method has been utilized within boundary condition. The rectangular region is split into mashes of line collateral to X and Y axis. Here we consider X axis analogous to plate and Y axis perpendicular to the plate as shown in figure 2. Height of the plate is $X_{\max}=30$ i.e. X changes from 0 to 30 and regard $Y_{\max}=50$ i.e. changes from 0 to 50. The grid spacing are $m=200$ in X direction and $n=300$ in Y direction. It is considered that ΔX and ΔY be constant lattice area toward X and Y ways respectively and conclude as $\Delta X=0.15\left(0\le X\le 30\right)$ and $\Delta Y=0.17\left(0\le Y\le 50\right)$ with small time step $\Delta\tau=0.001$. Let U',V',θ' and ϕ' depicts the value of U,V,θ and ϕ at end of time step respectively.

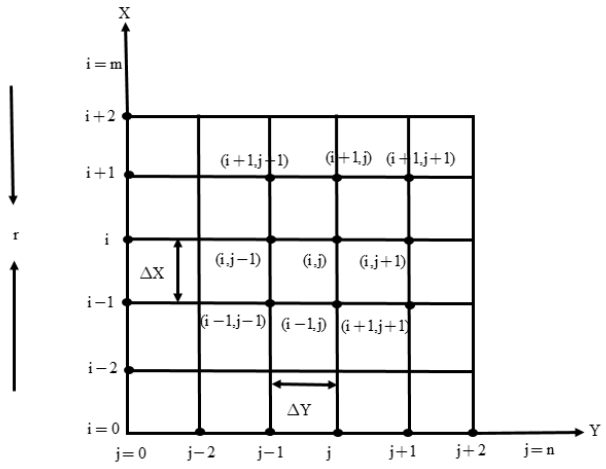

Figure 2. Finite difference space grid

Applying explicit finite difference method equations (8) to (12) are solved numerically and given below

Continuity equation:

$$\frac{U_{i,j}-U_{i-1,j}}{\Delta X}+\frac{V_{i,j}-V_{i,j-1}}{\Delta Y}=0 \tag{13}$$

Momentum Equation:

$$\begin{aligned} &\frac{U'_{i,j}-U_{i,j}}{\Delta\tau}+U_{i,j}\frac{U_{i,j}-U_{i-1,j}}{\Delta X}+V_{i,j}\frac{U_{i,j+1}-U_{i,j}}{\Delta Y}\\ &=\left[1+We\frac{U_{i,j+1}-U_{i,j}}{\Delta Y}\right]\left(\frac{U_{i,j+1}-2U_{i,j}+U_{i,j-1}}{(\Delta Y)^2}\right)\\ &-\left[M+\frac{1}{Da}\right]U_{i,j}+Gr\,\theta_{i,j}+Gm\,\phi_{i,j} \end{aligned} \tag{14}$$

$$\begin{aligned} &\frac{\theta'_{i,j}-\theta_{i,j}}{\Delta\tau}+U_{i,j}\frac{\theta_{i,j}-\theta_{i-1,j}}{\Delta X}+V_{i,j}\frac{\theta_{i,j+1}-\theta_{i,j}}{\Delta Y}\\ &=\frac{1}{\Pr}\left[1+\frac{4R}{3}\right]\left(\frac{\theta_{i,j+1}-2\theta_{i,j}+\theta_{i,j-1}}{(\Delta Y)^2}\right)\\ &+Ec\left(\frac{U_{i,j+1}-U_{i,j}}{\Delta Y}\right)^2+We.Ec.\left(\frac{U_{i,j+1}-U_{i,j}}{\Delta Y}\right)^3-M.Ec.\left(U_{i,j}\right)^2 \end{aligned} \tag{15}$$

Concentration Equation:

$$\begin{aligned} &\frac{\phi'_{i,j}-\phi_{i,j}}{\Delta\tau}+U_{i,j}\frac{\phi_{i,j}-\phi_{i-1,j}}{\Delta X}+V_{i,j}\frac{\phi_{i,j+1}-\phi_{i,j}}{\Delta Y}\\ &=\frac{1}{Sc}\left[\frac{\phi_{i,j+1}-2\phi_{i,j}+\phi_{i,j-1}}{(\Delta Y)^2}\right]+Sr\left[\frac{\theta_{i,j+1}-2\theta_{i,j}+\theta_{i,j-1}}{(\Delta Y)^2}\right]-Kc\,\phi_{i,j} \end{aligned} \tag{16}$$

The Corresponding boundary condition:

$$U_{i,0}^{n}=1,\ \theta_{i,0}^{n}=1,\ \phi_{i,0}^{n}=1 \qquad (17)$$
$$U_{i,L}^{n}=0,\ \theta_{i,L}^{n}=0,\ \phi_{i,L}^{n}=0 \quad where\, L\to\infty$$

Where, i and j designates mesh points toward X and Y axis respectively and n indicates magnitude of time, $\tau=n\Delta\tau$, here n=0,1,2,3,…

4. Stability and Convergence Analysis

The investigation of the problem will imperfect except we examine the stability of explicit finite difference technique. At time τ, the Fourier expansion for the common term U,θ and ϕ are

$$U:\psi(\tau)e^{i\alpha X}e^{i\beta Y},\ \theta:\xi(\tau)e^{i\alpha X}e^{i\beta Y},\ \phi:\varphi(\tau)e^{i\alpha X}e^{i\beta Y} \qquad (18)$$

After a time step Fourier expansion for U,θ and ϕ will be

$$U:\psi'(\tau)e^{i\alpha X}e^{i\beta Y},\theta:\xi'(\tau)e^{i\alpha X}e^{i\beta Y},\ \phi:\varphi'(\tau)e^{i\alpha X}e^{i\beta Y} \qquad (19)$$

Substituting the expressions (18) and (19) into equations (13) to (16) and let U and V are constant through any time step, we get

Momentum Equation:

$$\frac{(\psi'-\psi)e^{i\alpha X}e^{i\beta Y}}{\Delta\tau}+U\frac{\psi\left(1-e^{-i\alpha\Delta X}\right)e^{i\alpha X}e^{i\beta Y}}{\Delta X} \qquad (20)$$
$$+V\frac{\psi\left(e^{i\beta\Delta Y}-1\right)e^{i\alpha X}e^{i\beta Y}}{\Delta Y}=Gr.\xi e^{i\alpha X}e^{i\beta Y}+Gm.\varphi e^{i\alpha X}e^{i\beta Y}$$
$$+\frac{2\psi(\cos\beta\Delta Y-1)e^{i\alpha X}e^{i\beta Y}}{(\Delta Y)^2}\left\{1+We\frac{\psi\left(e^{i\beta\Delta Y}-1\right)e^{i\alpha X}e^{i\beta Y}}{\Delta Y}\right\}$$
$$-\left(M+\frac{1}{Da}\right)\psi e^{i\alpha X}e^{i\beta Y}$$
$$\psi'=\psi\left[1+\frac{2\Delta\tau(\cos\beta\Delta Y-1)}{(\Delta Y)^2}\left\{1+2We\frac{\left(e^{i\beta\Delta Y}-1\right)}{\Delta Y}\right\}\right.$$
$$\left.-\left(M+\frac{1}{Da}\right)\Delta\tau-U\frac{\Delta\tau\left(1-e^{-i\alpha\Delta X}\right)}{\Delta X}-V\frac{\Delta\tau\left(e^{i\beta\Delta Y}-1\right)}{\Delta Y}\right]+Gr.\Delta\tau\xi+Gm.\Delta\tau\varphi$$

Or, $\psi'=A_1\psi+A_2\xi+A_3\varphi$

where, $A_1=1+\frac{2\Delta\tau(\cos\beta\Delta Y-1)}{(\Delta Y)^2}\left\{1+2We\frac{\left(e^{i\beta\Delta Y}-1\right)}{\Delta Y}\right\}$

$$-\left(M+\frac{1}{Da}\right)\Delta\tau-U\frac{\Delta\tau\left(1-e^{-i\alpha\Delta X}\right)}{\Delta X}-V\frac{\Delta\tau\left(e^{i\beta\Delta Y}-1\right)}{\Delta Y},\ A_2=Gr.\Delta\tau,$$

$A_2=Gr.\Delta\tau$, $A_3=Gm.\Delta\tau$

Energy Equation:

$$\frac{(\xi'-\xi)e^{i\alpha X}e^{i\beta Y}}{\Delta\tau}+U\frac{\xi\left(1-e^{-i\alpha\Delta X}\right)e^{i\alpha X}e^{i\beta Y}}{\Delta X}$$
$$+V\frac{\xi\left(e^{i\beta\Delta Y}-1\right)e^{i\alpha X}e^{i\beta Y}}{\Delta Y}=We.Ec.\frac{\psi\left(e^{i\beta\Delta Y}-1\right)^3e^{i\alpha X}e^{i\beta Y}}{(\Delta Y)^3}$$
$$+\frac{1}{\Pr}\left(1+\frac{4R}{3}\right)\frac{2\xi(\cos\beta\Delta Y-1)e^{i\alpha X}e^{i\beta Y}}{(\Delta Y)^2}+Ec\frac{\psi\left(e^{i\beta\Delta Y}-1\right)^2e^{i\alpha X}e^{i\beta Y}}{(\Delta Y)^2}-M.Ec.U^2$$
$$\text{Or},\xi'=\xi\left[1+\frac{1}{\Pr}\left(1+\frac{4R}{3}\right)\frac{2\Delta\tau(\cos\beta\Delta Y-1)}{(\Delta Y)^2}-U\frac{\Delta\tau\left(1-e^{-i\alpha\Delta X}\right)}{\Delta X}-V\frac{\Delta\tau\left(e^{i\beta\Delta Y}-1\right)}{\Delta Y}\right]$$
$$+\psi\left[Ec\frac{\Delta\tau\left(e^{i\beta\Delta Y}-1\right)^2}{(\Delta Y)^2}+We.Ec.\frac{\Delta\tau\left(e^{i\beta\Delta Y}-1\right)^3}{(\Delta Y)^3}-M.Ec.\Delta\tau U^2\right]$$

$$\text{Or, } \xi'=A_4\psi+A_5\xi+0.\varphi \qquad (21)$$

where,

$$A_4=Ec\frac{\Delta\tau\left(e^{i\beta\Delta Y}-1\right)^2}{(\Delta Y)^2}+We.Ec.\frac{\Delta\tau\left(e^{i\beta\Delta Y}-1\right)^3}{(\Delta Y)^3}-M.Ec.\Delta\tau U^2$$

$$A_5=1+\frac{1}{\Pr}\left(1+\frac{4R}{3}\right)\frac{2\Delta\tau(\cos\beta\Delta Y-1)}{(\Delta Y)^2}-U\frac{\Delta\tau\left(1-e^{-i\alpha\Delta X}\right)}{\Delta X}-V\frac{\Delta\tau\left(e^{i\beta\Delta Y}-1\right)}{\Delta Y}$$

Concentration Equation:

$$\frac{(\varphi'-\varphi)e^{i\alpha X}e^{i\beta Y}}{\Delta\tau}+U\frac{\varphi\left(1-e^{-i\alpha\Delta X}\right)e^{i\alpha X}e^{i\beta Y}}{\Delta X}$$
$$+V\frac{\varphi\left(e^{i\beta\Delta Y}-1\right)e^{i\alpha X}e^{i\beta Y}}{\Delta Y}=-Kc.\varphi e^{i\alpha X}e^{i\beta Y}$$
$$+\frac{1}{Sc}\frac{2\varphi(\cos\beta\Delta Y-1)e^{i\alpha X}e^{i\beta Y}}{(\Delta Y)^2}+Sr\frac{2\xi(\cos\beta\Delta Y-1)e^{i\alpha X}e^{i\beta Y}}{(\Delta Y)^2}$$
$$\text{Or},\varphi'=\varphi\left[1+\frac{1}{Sc}\frac{2\Delta\tau(\cos\beta\Delta Y-1)}{(\Delta Y)^2}-Kc.\Delta\tau\right.$$
$$\left.-U\frac{\Delta\tau\left(1-e^{-i\alpha\Delta X}\right)}{\Delta X}-V\frac{\Delta\tau\left(e^{i\beta\Delta Y}-1\right)}{\Delta Y}\right]+Sr\frac{2\Delta\tau(\cos\beta\Delta Y-1)}{(\Delta Y)^2}\xi$$

$$\text{Or, } \varphi'=0.\psi+A_6\xi+A_7.\varphi \qquad (22)$$

where, $A_6=Sr\frac{2\Delta\tau(\cos\beta\Delta Y-1)}{(\Delta Y)^2}$

$$A_7=1+\frac{1}{Sc}\frac{2\Delta\tau(\cos\beta\Delta Y-1)}{(\Delta Y)^2}-Kc.\Delta\tau$$
$$-U\frac{\Delta\tau\left(1-e^{-i\alpha\Delta X}\right)}{\Delta X}-V\frac{\Delta\tau\left(e^{i\beta\Delta Y}-1\right)}{\Delta Y}$$

The equations (25) to (27) can be expressed as matrix form

$$\begin{bmatrix}\psi'\\ \xi'\\ \varphi'\end{bmatrix}=\begin{bmatrix}A_1 & A_2 & A_3\\ A_4 & A_5 & 0\\ 0 & A_6 & A_7\end{bmatrix}\begin{bmatrix}\psi\\ \xi\\ \varphi\end{bmatrix}\Rightarrow \eta'=T\eta \Rightarrow \eta'=\begin{bmatrix}\psi'\\ \xi'\\ \varphi'\end{bmatrix} T=\begin{bmatrix}A_1 & A_2 & A_3\\ A_4 & A_5 & 0\\ 0 & A_6 & A_7\end{bmatrix} \eta=\begin{bmatrix}\psi\\ \xi\\ \varphi\end{bmatrix}$$

To get stability criterion, eigenvalues of the matrix T should be obtained. Time step $\Delta\tau$ is very small in explicit finite difference method i.e. tends to zero. Under this presumption, we have $A_2\to 0, A_3\to 0, A_4\to 0, A_6\to 0$ and the matrix T becomes, $T=\begin{bmatrix}A_1 & 0 & 0\\ 0 & A_5 & 0\\ 0 & 0 & A_7\end{bmatrix}$. Eigen values of the matrix T are $\lambda_1=A_1, \lambda_2=A_5, \lambda_3=A_7$. Each eigenvalues must not passed unity in modulus in stability analysis. Under this deliberation the stability conditions may be formulated as $|A_1|\le 1, |A_5|\le 1, |A_7|\le 1$. For convergence analysis, let

$a_1=\Delta\tau, b_1=U\frac{\Delta\tau}{\Delta X}, c_1=|-V|\frac{\Delta\tau}{\Delta X}, d_1=2\frac{\Delta\tau}{(\Delta Y)^2}$ and $f_1=\frac{\Delta\tau}{\Delta Y}$, here, $a_1, b_1, c_1, d_1$and f_1 are all real and nonnegative. Everywhere U is nonnegative and V is negative. The maximal modulus occurs at $\alpha\Delta X=m\pi$ and $\beta\Delta Y=n\pi$, where m and n are integer. Hence,

$$A_1=1+2f_1(\cos\beta\Delta Y-1)+2We\{\psi(\cos\beta\Delta Y-1)e^{i\alpha x}e^{i\beta Y}\}d_1$$
$$-\left(M+\frac{1}{Da}\right)a_1-(1-e^{-i\alpha\Delta X})b_1+(e^{i\beta\Delta Y}-1)c_1$$
$$A_5=1+\frac{1}{\Pr}\left(1+\frac{4R}{3}\right)(\cos\beta\Delta Y-1)d_1-(1-e^{-i\alpha\Delta X})b_1+(e^{i\beta\Delta Y}-1)c_1$$
$$A_7=1+\frac{1}{Sc}(\cos\beta\Delta Y-1)d_1-Kc.a_1-(1-e^{-i\alpha\Delta X})b_1+(e^{i\beta\Delta Y}-1)c_1$$

Now, simplifying the above equations

$$A_1=1-2\left[2f_1+2.We.d_1+\left(M+\frac{1}{Da}\right)\frac{a_1}{2}+b_1+c_1\right], A_5=1-2\left[\frac{1}{\Pr}\left(1+\frac{4R}{3}\right)d_1+b_1+c_1\right]$$
$$A_5=1-2\left[\frac{1}{\Pr}\left(1+\frac{4R}{3}\right)d_1+b_1+c_1\right]$$
$$A_7=1-2\left[\frac{1}{Sc}d_1+\frac{a_1}{2}Kc+b_1+c_1\right]$$

The maximum negative values of A_1, A_5 and A_7 are -1. Hence the stability conditions are

$$U\frac{\Delta\tau}{\Delta X}+|V|\frac{\Delta\tau}{\Delta Y}+\frac{2\Delta\tau}{\Delta Y}+We\frac{2\Delta\tau}{(\Delta Y)^2}+\left(M+\frac{1}{Da}\right)\frac{\Delta\tau}{2}\le 1$$
$$U\frac{\Delta\tau}{\Delta X}+|V|\frac{\Delta\tau}{\Delta Y}+\frac{1}{\Pr}\left(1+\frac{4R}{3}\right)\frac{2\Delta\tau}{(\Delta Y)^2}\le 1$$
$$U\frac{\Delta\tau}{\Delta X}+|V|\frac{\Delta\tau}{\Delta Y}+\frac{1}{Sc}\frac{2\Delta\tau}{(\Delta Y)^2}+\frac{\Delta\tau Kc}{2}\le 1$$

From initial boundary conditions $U=V=T=0$, $\Delta\tau=0.001$, $\Delta x=0.15$ and $\Delta Y=0.17$, then the problem will be converged at $\Pr\ge 0.09$ and $Sc\ge 0.03$.

5. Results and Discussion

Two dimensional unsteady magneto-hydrodynamics boundary layer of multiphase fluid flow over a stretching or shrinking sheet has been investigated. In this section, the outcome of the problem is debated which have been found by enticing explicit finite difference method. The suitable values of the physical parameters are chosen as: $Gr=5$, $Gm=5$, $Sc=1.0$, $Sr=2.0$, $\Pr=0.71$, $R=2.50$, $We=0.10$, $Kc=1.50$, $Ec=0.50$, $Da=1$, $M=1$ for accuracy of the results. The above mentioned parameters effects on velocity, temperature as well as concentration profiles are expressed below.

Figure 3 represent the impact of modified Grashof number (*Gm*) on velocity outlines. Velocity increases at a proportional rate with modified Grashof number. So increasing value of modified Grashof number proliferates thermal elasticity force and high elasticity force increase velocity. The influence of the velocity distributions of thermal Grashof number (*Gr*) is discussed in Figure 4. Thermal buoyancy force increase the gravitational force which stem liquid particles for this reason velocity increase. The effect of different values of radiation parameter (*R*) on velocity profile is shown with the help of Figure 5. It is apparent that velocity has upswing tendency with increasing value of radiation parameter. Figure 6 reveal the influence of the changing the values of radiation parameter on temperature outline. Radiation is a heat transfer process which emits the energy through fluid particle. Hence temperature distribution increases for high values of radiation parameter. Figure 7 exhibits the impact of concentration outlines due to numerous magnitudes of Schmidt number (*Sc*). It is noticed that concentration profiles decrease at each point of flow field with higher value of Schmidt number because Schmidt number is the ratio of the momentum diffusivity to mass diffusivity. The plots of Prandtl number (*Pr*) on temperature profile is portrayed in Figure 8. With rising value of Prandtl number, thermal boundary layer thickness reduces. Physically at high Prandtl number fluid has a narrow thermal boundary layer and this enlarges the gradient of temperature. Figure 9 depicts the concentration field due to numerous magnitudes of Soret number (*Sr*). Concentration profiles expand with soar of Soret number. The influence of velocity distribution is presented for magnetic factor (*M*) in Figure 10. Physically, the presence of transverse magnetic field

introduces a Lorentz force that results in delay on the velocity field. The concentration circulation for numerous values of chemical reaction parameter (*Kc*) is introduced in Figure 11. Physically the chemical reaction parameter unveils a destructive reaction for positive values and this destructive reaction leads to decrease in concentration field that result in fails the buoyancy effect for concentration gradient. Figure 12 and 13 introduce velocity and temperature profiles for various numerical values of Weissenberg number (*We*). The observation from the figure is that initially velocity profile increases for large value of Weissenberg number but at a point, the velocity curve decreases. On the other hand, for increasing value of Weissenberg number, the thermal boundary layer decreases. The temperature outlines for various values of Eckert number *Ec* is portrayed in Figure 14. Higher Eckert number lessen width of thermal boundary layer that's why temperature of the fluid decreases.

Table 1. Comparison table for *Gm* on velocity field, *U* at y= 0.83136 when, *Gr*=5.0, *R*=1.0, *Sc*=0.60, *Pr*=0.71, K_r=0.6, *M*=1.0, *Sr*= 0.o and *We*= 0.0.

Parameter	Previous Results [27]	Present Results
Gm= 5.0	2.53247	2.54321
Gm= 10.0	3.72613	3.72515
Gm= 15.0	5.15284	5.17531
Gm= 20.0	6.35522	6.35267

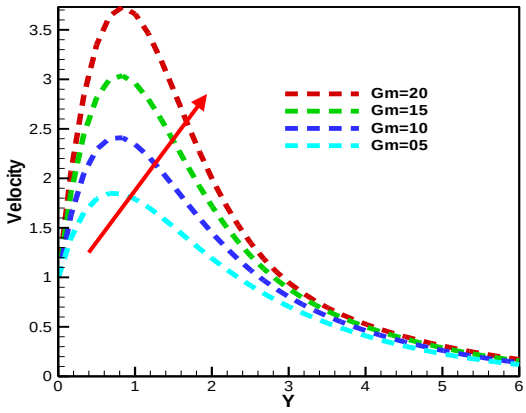

Figure 3. Effect of modified Grashof number *Gm* on velocity profiles.

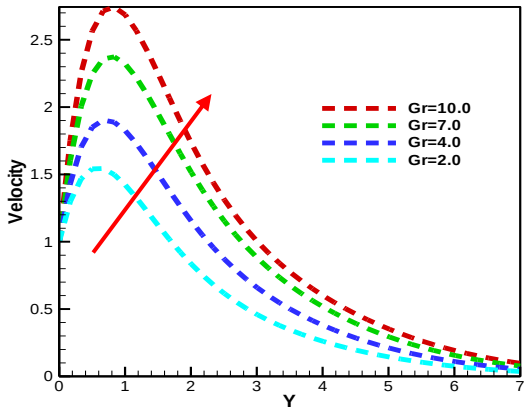

Figure 4. Effect of thermal Grashof number *Gr* on velocity profiles.

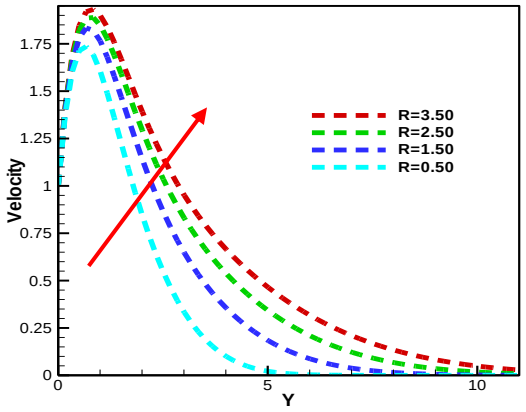

Figure 5. Effect of radiation parameter *R* on velocity profiles.

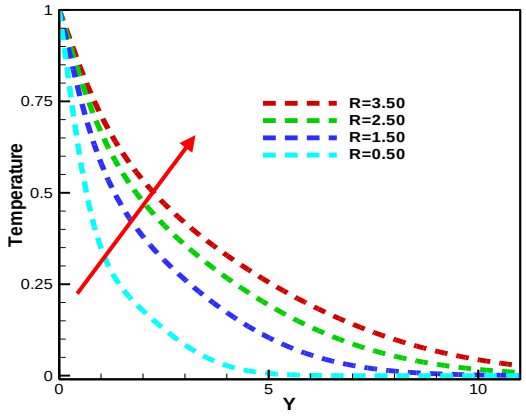

Figure 6. Effect of radiation parameter *R* on temperature profiles.

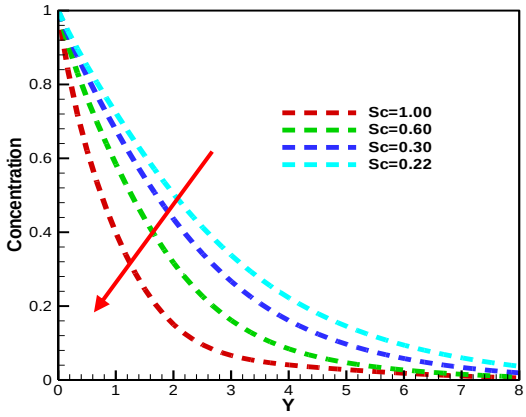

Figure 7. Effect of Schmidt number *Sc* on concentration profiles.

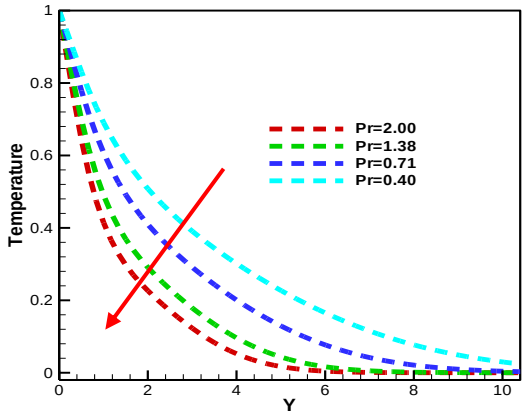

Figure 8. Effect of Prandtl number *Pr* on temperature profiles

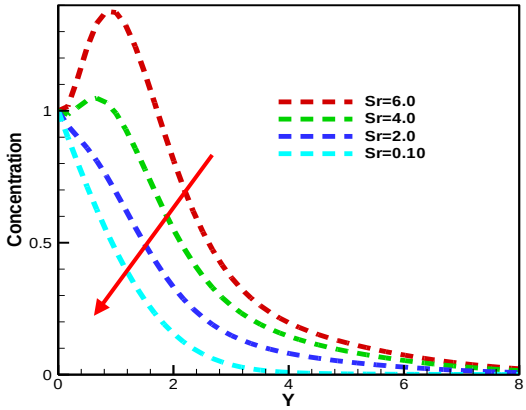

Figure 9. Effect of soret number *Sr* on concentration profiles.

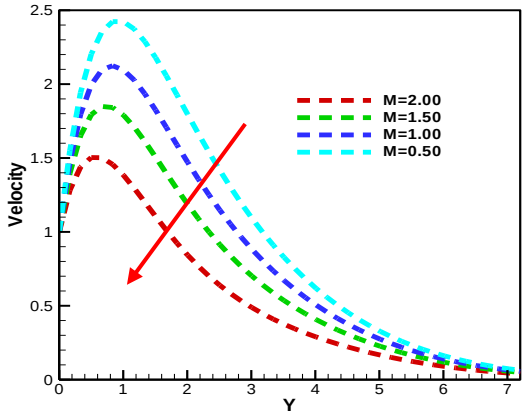

Figure 10. Effect of magnetic parameter *M* on velocity profiles.

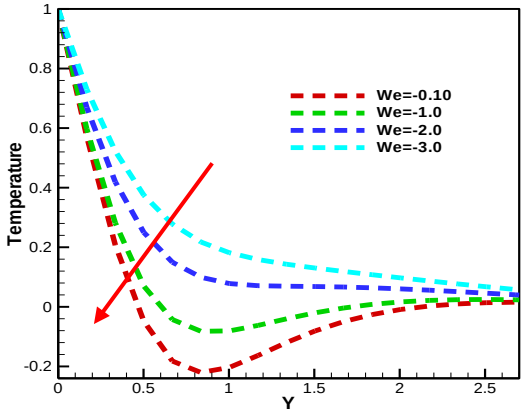

Figure 11. Effect of Weissenberg number *We* on temperature profiles.

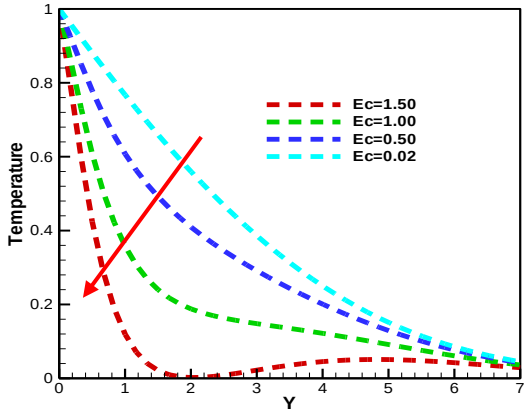

Figure 12. Effect of Eckert number *Ec* on velocity profiles.

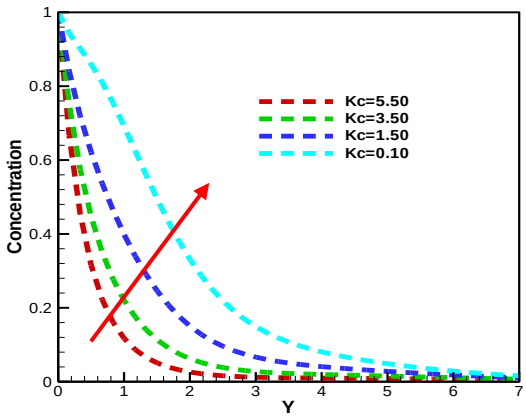

Figure 13. Effect of chemical reaction parameter *Kc* on concentration profiles.

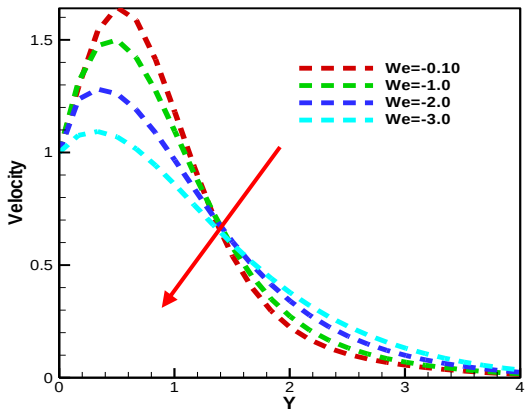

Figure 14. Effect of Weissenberg number *We* on velocity profiles.

Table 2. Variation of physical parameter (*Sc*, *Da*, *Gr* and *Ec*) on skin friction, Nusselt number and Sherwood number.

Sc	*Da*	*Gr*	*Ec*	*Cf*	*Nu*	*Sh*
0.22				0.69933	0.22462	0.14454
0.30				0.68689	0.21501	0.17634
0.60				0.65964	0.20084	0.24885
	1.0			0.29226	0.14963	0.45291
	2.0			0.44804	0.16785	0.44827
	3.0			0.59544	0.18497	0.45416
		2.0		0.91099	0.31836	0.89798
		4.0		0.76386	0.21595	0.53987
		7.0		0.69291	0.16125	0.37604
			0.02	0.61221	0.10040	0.49841
			0.50	0.59544	0.18497	0.45416
			1.00	0.56963	0.33545	0.35032

Figure 15 depicts the streamlines line view for Schmidt number $Sc = 0.22$ and $Sc = 0.30$. Streamlines flood view for $Sc = 0.22$ and $Sc = 0.30$ are showed in Figure 16. It is noted from streamlines profile that the streamlines fall down due to higher values of Schmidt number. Figure 17 and 18 represent the isotherm line view and flood view for magnetic parameter $M = 1$ and $M = 2.0$ respectively. Isotherm declines for growing magnitudes of magnetic parameter. Additionally, the impact of several physical parameters are discussed on skin friction, heat transfer rate and mass transfer rate profiles. The results are self-evident in Table 2 and Table 3. Furthermore, a numerical validation has been depicted in Table 1 and an excellent agreement with previously published papers is visible there.

Table 3. Variation of physical parameter (*R*, *Sr*, *We* and *Gm*) on skin friction, Nusselt number and Sherwood number.

R	*Sr*	*We*	*Gm*	*Cf*	*Nu*	*Sh*
0.50				0.56638	0.35250	0.31043
1.50				0.59107	0.20035	0.44344
2.50				0.60561	0.15436	0.47356
	0.10			0.62681	0.17984	0.25759
	2.0			0.68029	0.19337	0.16078
	4.0			0.74264	0.20685	0.08504
		-1.00		0.48882	1.12711	-7.9490
		-2.00		0.41726	0.93632	-6.7155
		-3.00		0.13219	0.76065	-5.2428
			5.0	0.59544	0.18497	0.45416
			10.0	0.93357	0.19747	0.49117
			15.0	1.25304	0.18514	0.58363

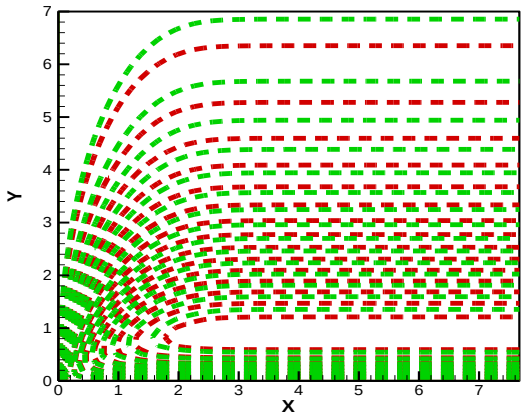

Figure 15. Streamlines line view when *Sc* = 0.30 (Red dash line) and *Sc*=0.22 (Green dash line).

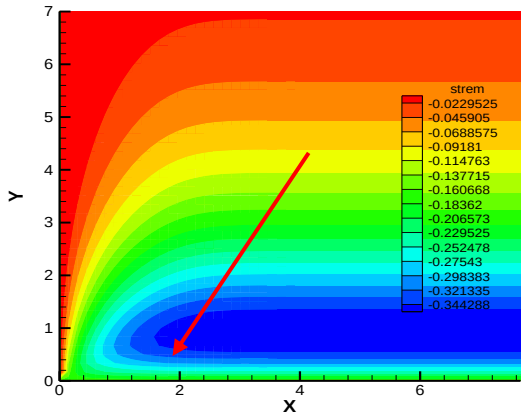

Figure 16. Streamlines flood view when *Sc* = 0.30 (Red dash line) and *Sc*=0.22 (Green dash line).

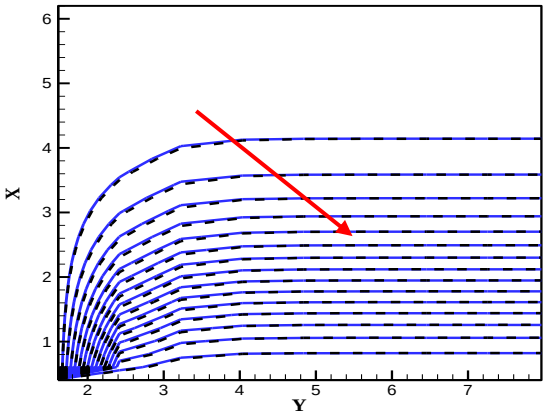

Figure 17. Isotherm line view when *M* = 2.0 (Blue dash line) and *M*=1.0 (Black dash line).

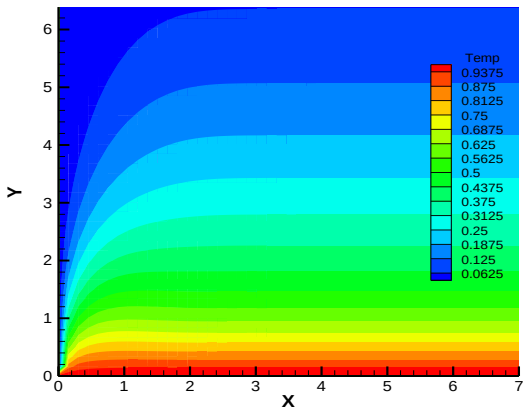

Figure 18. Isotherm flood view when *M* = 2.0 (Blue dash line) and *M*=1.0 (Black dash line).

6. Conclusions

The principal findings of our study are concluded as follows

- The velocity profile proliferates with growing values of thermal Grashof number (*Gr*), radiation parameter (*R*), soret number (*Sr*). On the other hand, velocity profile decreases for increasing values of Schmidt number (*Sc*), Prandtl number (*Pr*), magnetic parameter (*M*), chemical reaction parameter (*Kc*) and Eckert number (*Ec*).
- The Temperature distribution enhances for large values of radiation parameter (*R*) and Schmidt number (*Sc*) but shows decreasing curve for Weissenberg number (*We*), Prandtl number (*Pr*), soret number (*Sr*), magnetic parameter (*M*), Eckert number (*Ec*) and Darcy number (*Da*).
- The concentration outline reduces for higher values of chemical reaction parameter (*Kc*) and Schmidt number (*Sc*) whereas soret number upsurge.

References

Reza-E-Rabbi, S., Ahmmed, S. F., & Arifuzzaman, S. M. (2020). Computational modelling of multiphase fluid flow behavior over a stretching sheet in the presence of nanoparticles. *Engineering Science and Technology, an International Journal*, 23(3): 605-617.

Hayat, T., Shafiq, A., & Farooq, M. A. (2016). Newtonian and Joule heating effects in two-dimensional flow of Williamson fluid. *Journal of Applied Fluid Mechanics*, *9*(4): 1969-197.

Venkataramanaiah, G., SreedharBabu, Dr. M., & Lavanya, M. (2016). Heat generation/absorption effects on Magneto Williamson nanofluid flow with heat and mass fluxes. *International Journal of Engineering Development and Research*, *4*(1): 384-397.

Khan, M., Malik, M. Y., & Salahuddin, T. (2018). Heat and mass transfer of Williamson nanofluid flow yield by an inclined Lorentz force over a nonlinear stretching sheet. *Results in Physics*, *8*: 862-868.

Krisnamurthy, M. R., Prasannakumara, B. C., & Gireesha, B. J. (2015). Effect of chemical reaction on MHD boundary layer flow and melting heat transfer of Williamson nanofluid in porous medium. *Engineering Science and Technology*, *19*: 53-61.

Khan, M., Malik, M. Y., & Salahuddin, T. (2016). Heat transfer squeezed flow of Carreau fluid over a sensor surface with variable thermal conductivity: A numerical study. *Results in Physics*, *6*: 940-945.

Ali, L., Islam, S., & Gul, T. (2017). The Brownian and thermophoretic analysis of the non-Newtonian Willamson fluid flow of thin film in a porous space over an unstable stretching surface. *Applied science*, *7*: 404.

Reddy, J. V. R., Sugunamma, V., & Sandeep, N. (2017). Thermophoresis and Brownian motion effects on unsteady MHD nanofluid flow over a slandering stretching surface with slip effects. *Alexandria Engineering Journal*. Doi: 10.1016/j.aej.2017.02.014

Abah, S. O., Eletta, B. E., & Omale, S. O. (2012). The numerical analysis of the effect of free convection heat and mass transfer on the unsteady boundary layer flow past a vertical plate. *International Journal of Theoretical and Mathematical Physics*, *2*(3): 33-36.

Barik, R. N. (2016). Heat and mass transfer effects on unsteady MHD flow through an accelerated isothermal vertical plate embedded in porous medium in the presence of heat source and chemical reaction. *European Journal of Advances in Engineering and Technology*, *3*(1): 56-61.

Khan, Md. S., Alam, Md. M., & Tzirtzilakis, E. E. (2016). Finite difference simulation of MHD radiative flow of a nanofluid past a stetching sheet with stability analysis. *International Journal of Advanced Thermofluid Research*, *2*(1): 31-46.

Kataria, H. R., & Patel, H. R. (2016). Radiation and chemical reaction effects on MHD Casson fluid flow past an oscillating vertical plate embedded in porous medium. *Alexandria Engineering Journal*, *55*: 583-595.

Kataria, H. R., & Patel H. R. (2016). Soret and heat generation effects on MHD Casson fluid flow past an oscillating vertical plate embedded through porous medium. *Alexandria Engineering Journal*, *55*: 2125-2137.

Hussanan, A., Salleh, M. Z., & Tahar R. M. (2014). Unsteady boundary layer flow and heat transfer of a Casson fluid past an oscillating vertical plate with Newtonian heating, *PLOS ONE*, *9*(10): e108763.

Shaw, S., Mahanta, G., & Sibanda, P. (2016), Non-linear thermal convection in a Casson fluid flow over a horizontal plate with convective boundary condition. *Alexandria Engineering Journal*, *55*: 1295-1304.

Ramandevi, B., Reddy, J. V. R., & Sugunamma, V. (2017). Combined influenced of viscous dissipation and non-uniform heat source/sink on MHD non-Newtonian fluid flow with cattaneo-christov heat flux. *Alexandria Engineering Journal.* Doi: 10.1016/j.aej. 2017.01.026

EL-Naby, M. A. ABD, Elbarbary, E. M. E., & Abdelazem, N. Y. (2003). Finite difference solution of radiation effects on MHD unsteady free-convection flow over vertical plate with variable surface temperature. *Journal of Applied Mathematics*, *2*: 65-86.

Khan, M.S., Alam, M.M., Tzirtzilakis, E.E., Ferdows, M., Karim, I., (2016). Finite Difference Simulation of MHD Radiative Flow of a Nanofluid past a Stretching Sheet with Stability Analysis. *International Journal of Advanced Thermofluid Research*, 2: 31-46.

Loganathan, P. (2010). Effects of thermal conductivity on unsteady MHD free convective flow over a semi-infinite vertical plate. *International Journal of Engineering Science and Technology*, *2*(11): 6257-6268.

Hemalatha, E., & Reddy, N. B. (2014). Effect of thermal radiation on MHD free convection flow past a flat plate with convective surface boundary condition. *International Journal of Mathematical Archive*, *5*(10): 279-286.

Gaffar, S. A., Prasad, V. R., & Reddy, S. K. (2016). Magneto hydrodynamic free convection boundary layer flow of non-Newtonian tangent hyperbolic fluid from a vertical permeable cone with variable temperature. *Journal of the Brazilian Society of Mechanical Sciences and Engineering*. DOI: 10.1007/s40430-016-0611-x

Parveen, N., & Alim, M. A. (2012). Joule heating effect on magnetohydrodynamics natural convection flow along a vertical wavy surface. *Journal of Naval Architecture and Marine Engineering*, *9*: 11-24. DOI:10.3329/jname.v8i1.5954

Reza-E-Rabbi, S., Ahmmed, S. F., & Arifuzzaman, S. M. (2020). Explicit finite difference analysis of an unsteady MHD flow of a chemically reacting Casson fluid past a stretching sheet with Brownian motion and thermophoresis effects. *Journal of King Saud University*, *4*: 234-243.

Abro, K. A., Siyal, A., & Atangana, A. (2021). Thermal stratification of rotational second-grade fluid through fractional differential operators. *Journal of Thermal Analysis and Calorimetry*, 143(5): 3667-3676.

Nikan, O., Golbabai, A., Machado, J. A., & Nikazad, T. (2021). Numerical solution of the fractional Rayleigh–Stokes model arising in a heated generalized second-grade fluid. *Engineering with Computers*, 37(3): 1751-1764.

Gharami, P.P., Reza-E-Rabbi, S., Arifuzzaman, S.M., Khan, M.S., Sarker, T., Ahmmed, S.F. (2020a). MHD effect on unsteady flow of tangent hyperbolic nano-fluid past a moving cylinder with chemical reaction. *SN Applied Science.* 2**:** 1256.

Gharami, P.P., Arifuzzaman, S.M., Reza-E-Rabbi, S., Shakhaoath Khan, M., Ahmmed, S.F. (2020b). Analytical and numerical solution of viscous fluid flow with the effects of thermal radiation and chemical reaction past a vertical porous surface. *International Journal of Heat and Technology*, 38(3): 689-700.